1521-0111/83/2/354–366$25.00
MOLECULAR PHARMACOLOGY
http://dx.doi.org/10.1124/mol.112.081794
Mol Pharmacol 83:354–366, February 2013

Noncompetitive, Voltage-Dependent NMDA Receptor Antagonism by Hydrophobic Anions

Andrew J. Linsenbardt, Mariangela Chisari, Andrew Yu, Hong-Jin Shu, Charles F. Zorumski, and Steven Mennerick

Department of Psychiatry (A.J.L, A.Y.,H-J. S., C.F.Z., S.M.), Taylor Family Institute for Innovative Psychiatric Research (C.F.Z., S.M.), Department of Anatomy & Neurobiology (C.F.Z., S.M.), Washington University School of Medicine, St. Louis, Missouri; and Department of Clinical and Molecular Biomedicine (M.C.), Section of Pharmacology and Biochemistry, University of Catania, Catania, Italy

Received August 10, 2012; accepted November 9, 2012

ABSTRACT

NMDA receptor (NMDAR) antagonists are dissociative anesthetics, drugs of abuse, and are of therapeutic interest in neurodegeneration and neuropsychiatric disease. Many well-known NMDAR antagonists are positively charged, voltage-dependent channel blockers. We recently showed that the hydrophobic anion dipicrylamine (DPA) negatively regulates $GABA_A$ receptor function by a mechanism indistinguishable from that of sulfated neurosteroids. Because sulfated neurosteroids also modulate NMDARs, here we examined the effects of DPA on NMDAR function. In rat hippocampal neurons DPA inhibited currents gated by 300 μM NMDA with an IC_{50} of 2.3 μM. Neither onset nor offset of antagonism exhibited dependence on channel activation but exhibited a noncompetitive profile. DPA antagonism was independent of NMDAR subunit composition and was similar at extrasynaptic and total receptor populations. Surprisingly, similar to cationic channel blockers but unlike sulfated neurosteroids, DPA antagonism was voltage dependent. Onset and offset of DPA antagonism were nearly 10-fold faster than DPA-induced increases in membrane capacitance, suggesting that membrane interactions do not directly explain antagonism. Furthermore, voltage dependence did not derive from association of DPA with a site on NMDARs directly accessible to the outer membrane leaflet, assessed by DPA translocation experiments. Consistent with the expected lack of channel block, DPA antagonism did not interact with permeant ions. Therefore, we speculate that voltage dependence may arise from interactions of DPA with the inherent voltage dependence of channel gating. Overall, we conclude that DPA noncompetitively inhibits NMDA-induced current by a novel voltage-dependent mechanism and represents a new class of anionic NMDAR antagonists.

Introduction

NMDA receptors (NMDARs) have been the object of intense investigation for more than three decades. NMDAR channels exhibit gating contingent on both agonist binding and on membrane potential. As such, NMDARs are molecular coincidence detectors of presynaptic glutamate release and postsynaptic activity (Dingledine et al., 1999; Nakazawa et al., 2004). The voltage dependence of gating, along with Ca^{2+} permeability of the channels, imbues NMDARs with properties important for roles in synaptic development and neuroplasticity (Lu et al., 2001; Collingridge et al., 2004).

NMDARs exhibit several forms of voltage-dependent modulation. Although Mg^{2+} block of the channel is the major source of physiologic NMDAR voltage dependence, NMDARs also exhibit inherent voltage-dependent gating, independent of Mg^{2+} block (Jahr and Stevens, 1990; Nowak and Wright, 1992; Clarke and Johnson, 2008) that could be subject to regulation or modulation. This direct effect of voltage on channel gating is much more subtle than Mg^{2+} block but is a common feature of many other ligand-gated channels including AMPA (Boulter et al., 1990), $GABA_A$ (Weiss, 1988), glycine (Jin et al., 2009), and nicotinic receptors (Anderson and Stevens, 1973). Similar to Mg^{2+} effects on NMDAR channels, several hydrophobic cationic drugs block NMDAR activity through voltage-dependent interaction with the open channel. These include dissociative anesthetics with both therapeutic and abuse potential [e.g., ketamine (Ketaset), memantine (Namenda), phencyclidine (PCP), [5*R*,10*S*]-[+]-5-methyl-10,11-dihydro-5*H*-dibenzo[a,d]cyclohepten-5,10-imine] (MK-801)] and tetraalkylammonium compounds (Sobolevsky et al., 1999). These agents exhibit voltage dependence that is explained by the positive charge of the drug moving through a fraction of the transmembrane voltage difference to block the pore (Woodhull, 1973). Channel blockers can also be influenced by permeant ions and by mutation of amino acid residues in the pore region, confirming their access to the

This work was supported by the Bantly Foundation; the National Institutes of Health National Institute on Drug Abuse [Grant DA07261]; the National Institutes of Health National Institute of Mental Health [Grants MH078823 and MH 077791]; the National Institutes of Health National Institute on Alcohol Abuse and Alcoholism [Grant AA017413]; the National Institutes of Health National Institute of General Medical Sciences [Grant GM47969]; and the International Promotion of Young Researchers "Montalcini Program," sponsored by the Italian Ministry of Education, University and Research.
dx.doi.org/10.1124/mol.112.081794.

ABBREVIATIONS: DPA, dipicrylamine; HEK, human embryonic kidney; MK-801, [5R,10S]-[+]-5-methyl-10,11- dihydro-5H-dibenzo[a,d]cyclohepten-5,10-imine; NMDA, *N*-methyl-D-aspartate; TPB, tetraphenylborate; 3α5βS, 3α-hydroxy-5β-pregnan-20-one sulfate.

channel (MacDonald et al., 1987; Antonov et al., 1998; Antonov and Johnson, 1999; Kashiwagi et al., 2002).

Here we describe the first of a new class of anionic voltage-dependent modulators of NMDAR function. We recently showed that hydrophobic anions, used for decades as biophysical probes of membrane structure, are potent, use-dependent antagonists of $GABA_A$ receptor ($GABA_AR$) function (Chisari et al., 2011). Dipicrylamine (DPA), for instance, is one of the most potent antagonists of $GABA_A$Rs described. Because DPA is used as a probe of neuronal excitability, there is interest in whether it interacts with other ion channels that affect excitability. DPA's mechanism of action at $GABA_A$Rs is indistinguishable from that of sulfated neurosteroids that also modulate NMDARs and, like DPA, are lipophilic, negatively charged molecules. Thus, we were prompted to carry out the present investigation of NMDAR sensitivity to the DPA.

DPA and related compounds are unique probes of ion channel function because their interaction with the plasma membrane can be monitored electrically, through membrane capacitance measurements, or optically. This allows membrane interactions to be compared directly with properties of receptor modulation. As an anion, DPA accumulates in the inner membrane surface at positive membrane potentials and in the outer membrane surface at negative membrane potentials (Ketterer et al., 1971; Benz et al., 1976). Because of this voltage-dependent translocation, we may be able to gain insights into the receptor sites with which DPA interacts.

Like several sulfated neurosteroids, we found that the hydrophobic, anionic membrane probes DPA and tetraphenylborate (TPB) antagonize NMDAR function. Surprisingly, however, our results show that unlike sulfated neurosteroids, DPA and TPB exhibit voltage-dependent antagonism that is superficially similar to cationic pore blockers. We initially hypothesized that the voltage dependence arises from an external receptor binding site, coupled with the well characterized translocation of DPA to the inner membrane surface at positive membrane potentials. Instead, our work shows that antagonism does not correlate with voltage-dependent membrane retention or with the kinetics of membrane partitioning and departitioning. Rather, the off rate of DPA's antagonism is slower at negative potentials, possibly suggesting that DPA interacts with the intrinsic voltage-dependent gating of NMDAR channels. In summary, voltage-sensitive antagonism by DPA arises through a mechanism unrelated to the well characterized interaction of DPA with membrane bilayers.

Materials and Methods

Hippocampal Cultures. All animal care and experimental procedures were consistent with National Institutes of Health guidelines, approved by the Washington University Animal Studies Committee, and were similar to previously published methods (Mennerick et al., 1995). Hippocampal neurons were obtained from 1 to 3 day postnatal Sprague-Dawley rats anesthetized with isofluorane. After rats were decapitated, hippocampi were removed, cut into 500-μm-thick slices, and digested with 1 mg/ml papain in oxygenated Leibovitz L-15 medium (Life Technologies, Gaithersburg, MD). Tissue was mechanically dissociated in modified Eagle's medium (Life Technologies) containing 5% horse serum, 5% fetal calf serum, 17 mM D-glucose, 400 μM glutamine, 50 U/ml penicillin, and 50 μg/ml streptomycin. Cells were plated in modified Eagle's medium at a density of ~650 cells/mm^2 as mass cultures onto 25-mm coverslips coated with 5 μg/cm^2 poly-D-lysine and 1.7 μg/cm^2 laminin, or were plated as "microisland" cultures for autaptic recordings at a density of ~100 cells/mm^2 onto 35 mm plastic culture dishes stamped with collagen microdroplets on a layer of 0.15% agarose. Cytosine arabinoside (6.7 μM) was added 3–4 days after plating to arrest glial proliferation, and one-half the culture medium was replaced with Neurobasal medium (Life Technologies) containing 500 μM glutamine, 50 U/ml penicillin, 50 μg/ml streptomycin and B27 supplement (Life Technologies) 4–5 days after plating.

Xenopus Oocytes. cRNA encoding rat NMDAR subunits was injected into stage V–VI oocytes harvested from sexually mature female *Xenopus laevis* frogs (*Xenopus* 1, Northland, MI). Frogs were anesthetized with 0.1% tricane (3-aminobenzoic acid ethyl ester) during a partial ovariectomy. Oocytes were defolliculated by shaking for 20 minutes at 37°C in 2 mg/ml collagenase dissolved in a calcium-free solution containing (in mM) 96 NaCl, 2 KCl, 1 $MgCl_2$, and 5 *N*-(2-hydroxyethyl)piperazine-*N*′-ethanesulfonic acid (HEPES), pH 7.4. Capped RNA for GluN1a and GluN2A subunits was prepared in vitro (mMESSAGE mMachine kit, Ambion, Austin, TX) from linearized pBluescript vectors. Subunit RNA was injected in equal parts (50 ng of total RNA). After injection, oocytes were incubated at 18°C in ND96 solution containing (in mM) 96 NaCl, 2 KCl, 2 $CaCl_2$, 1 $MgCl_2$, and 5 HEPES, pH 7.4. ND96 was supplemented with pyruvate (5 mM), penicillin (100 U/ml), streptomycin (100 μg/ml), and gentamycin (50 μg/ml).

Human Embryonic Kidney Cell Transfection. HEK 293 cells were grown in Dulbecco's modified Eagle's medium (Life Technologies) with 10% fetal bovine serum and 1 mM glutamine in 35-mm culture dishes. Cells were transfected with wild-type GluN1a subunits along with wild-type GluN2A, GluN2B, GluN2C, or GluN2D subunits using Lipofectamine2000 (Life Technologies) according to the manufacturer's protocol. GluN2A subunits were packaged in pRc/CMV vectors; GluN2B subunits were packaged in a pcDNA1 vector; GluN2C subunits were packaged in pRKW2 vector; and GluN2D subunits were packaged in pCIneo KE vector. DsRed or eGFP was used as a positive transfection marker. Each dish was transfected with 0.3 μg GluN1a, 1 μg GluN2 (A-D) subunit, and 0.05 μg fluorescent protein cDNA. Following transfection, 300 μM ketamine was added to the medium to prevent excitotoxic cell death (Boeckman and Aizenman, 1996). Electrophysiology was performed 36–72 hours following transfection.

Electrophysiology. Whole cell recordings and capacitance estimates from neuronal cultures were performed 3–12 days following plating using an Axopatch 200B amplifier (Molecular Devices, Sunnyvale, CA). Whole cell recordings were obtained from transfected HEK cells under similar conditions. For recordings, cells were perfused with extracellular solution containing (in mM) 138 NaCl, 4 KCl, 2 $CaCl_2$, 10 glucose, 10 HEPES at pH 7.25. Patch pipettes were filled with solution containing (in mM) 130 cesium methanesulfonate, 4 NaCl, 10 HEPES, 0.5 $CaCl_2$, and 5 EGTA at pH 7.25, unless otherwise indicated. When filled with this solution, pipette tip resistance was 3–6 MΩ. Cells were usually clamped at −70 mV or as indicated in figure legends. Membrane capacitance was estimated by examining the integrated capacitive current (sampled at 50 kHz at 10-kHz filter cutoff frequency) to 5- to 20-mV depolarizing or hyperpolarizing voltage pulses. Drugs were applied with a multibarrel, gravity-driven local perfusion system that provides a laminar local stream for solution exchanges. Most NMDA-containing solutions were applied in low Ca^{2+} saline (0.25–0.5 mM) to diminish Ca^{2+}-dependent desensitization (Clark et al., 1990; Tong et al., 1995) and were nominally devoid of Mg^{2+} and D-APV. The common tip was placed 0.5 mm from the center of the microscope field. Solution exchange times were 120 ± 14 ms (10–90% rise) estimated from junction current rises at the tip of an open patch pipette. Experiments were performed at room temperature.

For isolation of extrasynaptic NMDARs, solitary neurons were grown on astrocyte islands (Mennerick et al., 1995). Autaptic, recurrent EPSCs were elicited with a brief depolarizing voltage pulse

(1.5 ms from −70 mV to +20 mV to elicit a breakaway presynaptic axonal action potential) in the presence of 10 μM MK-801 to selectively block postsynaptic NMDARs. Patch pipettes were filled with solution containing (in mM) 130 potassium gluconate, 2 NaCl, 0.1 EGTA, and 10 HEPES at pH 7.25. Alternatively, mass cultures were incubated for 15 minutes at 37°C in the presence of 50 μM bicuculline, 10 μM glycine, and 10 μM MK-801. We recently demonstrated that this protocol effectively blocks synaptic NMDARs in this preparation, yielding the expected ~70% inhibition of responses to exogenous NMDA (Wroge et al., 2012).

Oocyte responses to NMDA were recorded 2–5 days following RNA injection using a two-electrode voltage clamp (OC725C amplifier; Warner Instruments, Hamden, CT) at a membrane potential of −70 mV. The bath solution was ND96 solution with the following changes: Mg^{2+} was omitted, Ba^{2+} replaced Ca^{2+} to avoid activation of endogenous Ca^{2+}-dependent currents, and 10 μM glycine was added. Glass recording pipettes (~1 MΩ resistance) were filled with 3 M KCl. Compounds were applied to the oocytes using a multibarrel pipette with a common output tip. Data acquisition and analysis were performed with pCLAMP software (Molecular Devices). At the higher concentrations employed in this study (≥1 μM), DPA sometimes elicited a small D-APV insensitive inward steady current of unclear origin. To avoid confusing this effect with potentiation of NMDA responses, we preapplied DPA prior to coapplication with NMDA (e.g., Fig. 1), and for quantification we subtracted the DPA-induced current. The small current was inconsequential at high NMDA concentrations, which generated currents much larger than the DPA-induced current.

Data Analysis. Data acquisition and analysis were performed primarily using pCLAMP 10 software (Molecular Devices). Inhibition by antagonists was measured by quantifying the peak response to NMDA or, in the case of sustained antagonist application, by quantifying the average current during the final 50–100 ms of drug application. Extended analysis was done using Microsoft Excel (Microsoft, Redmond, WA) or GraphPad Prism (GraphPad Software, La Jolla, CA). Graphical figures and curve fitting were conducted with Clampfit (Molecular Devices) or SigmaPlot software (SPSS Science, Chicago, IL). Data are expressed as mean ± S.E.M. Statistical significance was determined using a Student's two-tailed *t*-test or two-way, repeated-measures analysis of variance, as indicated. Curve fitting of dose-response data was performed with the Hill equation $[I = I_{max} C^n / (EC_{50}{}^n + C^n)]$, where C is the agonist concentration, I_{max} is the maximum current amplitude, EC_{50} is the agonist concentration that yields a 50% response relative to I_{max}, and n is the Hill coefficient. Curve fits to the Boltzmann function were to an equation of the form $Y = Min+(Max-Min)/\{1+ \exp[(V_{1/2}-x)/S]\}$, where Min is the lower asymptote, Max is the upper asymptote, $V_{1/2}$ is the half-maximum voltage, and S is the slope factor (RT/zF).

Materials. All compounds were obtained from Sigma-Aldrich (St. Louis, MO) except for DPA, which was obtained from Biotium (Hayward, CA). DPA was supplied as DMSO stock or as powder from the supplier. We noticed no obvious differences in the behavior of several different DPA samples.

Results

DPA is Noncompetitive and Use Independent. We focused on DPA because we recently characterized it as a very potent, uncompetitive antagonist of $GABA_A$Rs and because it is a compound of interest as a probe of neuronal excitability (Chanda et al., 2005a,b; Bradley et al., 2009; Chisari et al., 2011). At $GABA_A$Rs, DPA exhibits similar antagonism to that

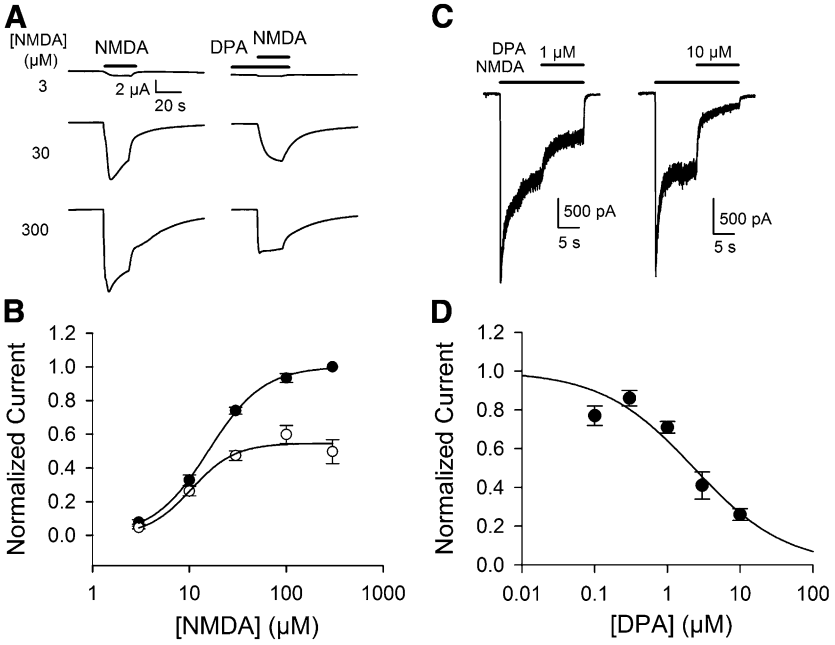

Fig. 1. DPA antagonism is potent and noncompetitive. (A) Current response in *Xenopus* oocytes injected with RNA encoding GluN1a/GluN2A subunits to NMDA (3, 30, and 300 μM; left) or a preapplication of DPA (5 μM) for 21 seconds followed by coapplication of DPA and NMDA (3, 30, and 300 μM; right) for 25 seconds. (B) NMDA concentration-response curve derived from oocytes exposed to NMDA alone (closed circles; $N = 7$), then to NMDA and DPA (open circles; $N = 7$) as in (A). Normalized peak current is plotted. Solid line represents fit to the Hill equation of the form $I = I_{max*} C^n/(EC_{50}{}^n + C^n)$, where I is measured current, I_{max} is maximum normalized current (relative to response at 300 μM), EC_{50} is the concentration of NMDA producing one-half the maximum response, C is agonist concentration, and n is the Hill coefficient. For fits to the closed circles, $I_{max} = 1.0$, $EC_{50} = 16 \pm 1.2$ μM, and $n = 1.5$. For fits to the open circles, $I_{max} = 0.55$, $EC_{50} = 12 \pm 2.1$ μM, and $n = 1.9$. The calculated EC_{50} values were significantly different ($P < 0.05$). (C) Current at −70 mV in a hippocampal neuron in response to NMDA (300 μM), followed by coapplication of NMDA and DPA (1 μM or 10 μM). (D) Inhibition curve derived from neurons administered NMDA (300 μM) and varied concentrations of DPA ($N = 5$–14). Steady-state current is plotted. Solid line represents a fit to the equation $I = I_{max*} C^n/(IC_{50}{}^n + C^n)$, where I_{max} is the maximum current, C is the test DPA concentration, n is the Hill coefficient, and IC_{50} is the concentration producing half inhibition. The IC_{50} was 2.3 μM, with a Hill coefficient (n) of 0.7.

of sulfated neurosteroids, which also modulate NMDARs (Park-Chung et al., 1997; Gibbs et al., 2006). To evaluate DPA effects on NMDARs, we first examined recombinant GluN1a/GluN2A NMDARs expressed in oocytes, where complete NMDA concentration-response curves could readily be obtained in the presence and absence of preapplied DPA (Fig. 1, A and B). This analysis showed that DPA exhibited a noncompetitive profile of antagonism, lowering the apparent efficacy (maximum responses) to NMDA but significantly reducing the NMDA EC_{50} (Fig. 1B). Subsequent experiments were performed in neurons and HEK cells to take advantage of more rapid drug delivery.

Hippocampal neurons exhibited somewhat higher sensitivity to DPA antagonism of NMDA currents. At a NMDA

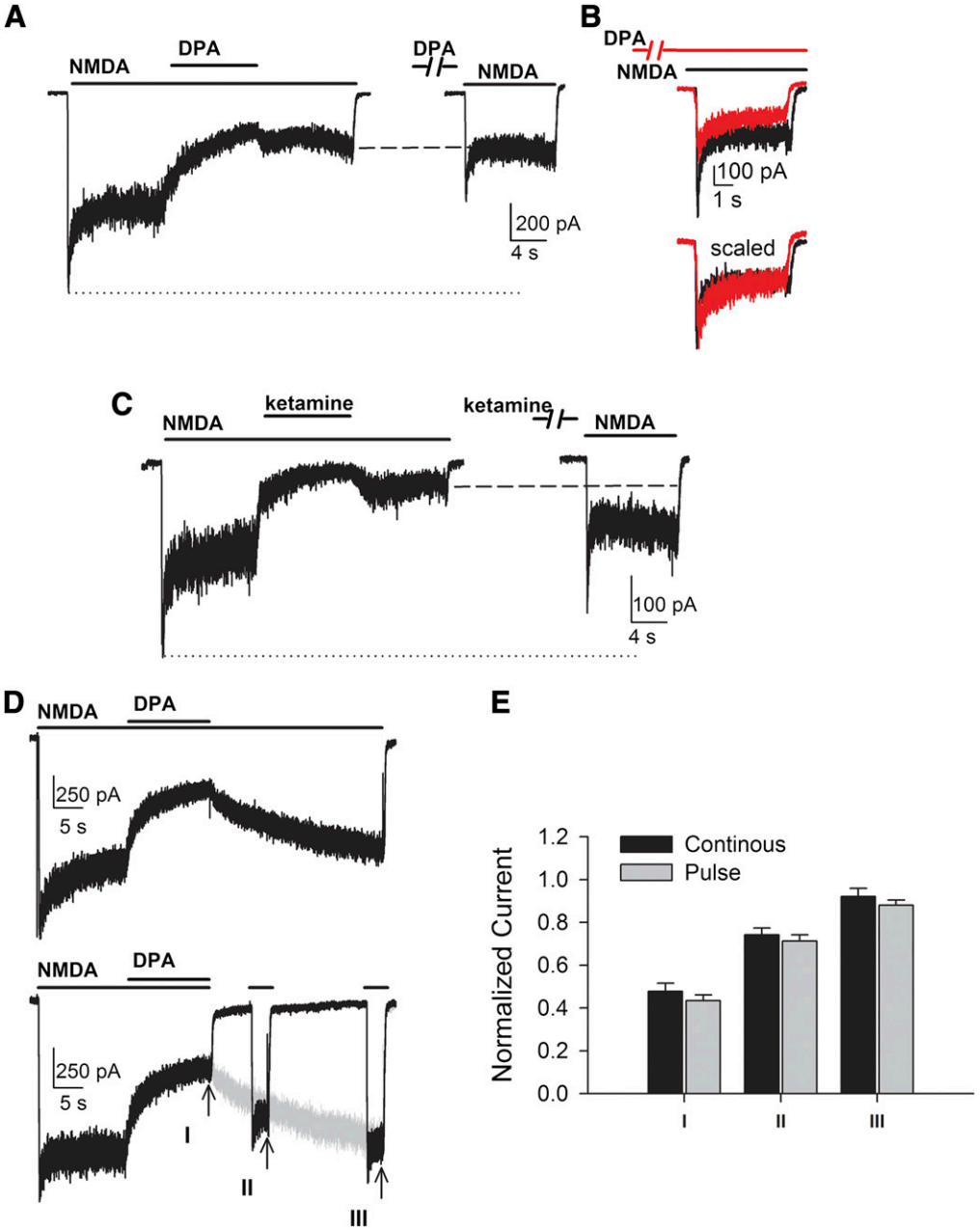

Fig. 2. Antagonism by DPA is not activation dependent. (A) Current response to NMDA (300 μM), then coapplication of DPA (2 μM), followed by a return to NMDA (left). After washing with BSA (0.1 mg/ml) to remove excess DPA and return the cell to control conditions, DPA (2 μM) was preapplied for 10 seconds, followed by NMDA alone (300 μM, right). (B) Neurons were administered NMDA alone (300 μM, black), then preapplied DPA (1 μM) for 10 seconds, then coapplied NMDA and DPA (red). Currents are overlaid to show inhibition by DPA (top), yet the level of inhibition of peak current and steady-state current are comparable when scaled (bottom). (C) Current response to NMDA (300 μM), then coapplication of ketamine (2.5 μM), then a return to NMDA (left). In the same cell, ketamine (2.5 μM) was preapplied for 10 seconds, followed by NMDA alone (300 μM, right). (D) Current response to NMDA (300 μM), then coapplication of DPA (3 μM), followed by a return to NMDA for 30 seconds (top). After removal of excess DPA with BSA (0.1 mg/ml), NMDA (300 μM) was reapplied, followed by coapplication of DPA (3 μM), then washout with saline and two 3-second pulses of NMDA (300 μM) to determine the degree of NMDAR current inhibition by DPA (bottom). The earlier wash application of NMDA is shown (gray trace) with the saline washout and NMDA pulses (black trace). Arrows depict the time point where current measurements were obtained under both treatments. (E) Average degree of inhibition of NMDA-induced current (300 μM) by DPA (3 μM; $N = 6$) at steady-state inhibition (I), then after 7 seconds (II), and 27 seconds (III) of continuous (black bars) wash with NMDA or pulses of NMDA (gray bars).

concentration of 300 μM, DPA exhibited an IC_{50} of 2.3 μM in dissociated cultures of postnatal rat hippocampal neurons (Fig. 1, C and D) and a higher IC_{50} of 15.7 ± 4.0 μM in *Xenopus* oocytes expressing GluN1/GluN2A NMDAR subunits (N = 6; data not shown). Whether this difference in sensitivity is related to NMDAR subunit composition or to cell type was addressed in ensuing experiments. In both cases, the IC_{50} was higher than that for antagonism of $GABA_A$Rs (Chisari et al., 2011), paralleling the difference in potency of neurosteroids at the two receptor types.

Despite superficial similarities to neurosteroids (noncompetitive antagonism, sensitivity of NMDARs and $GABA_A$Rs), the actions of DPA on NMDARs were distinct from at least some neurosteroid antagonists. For example, the neurosteroid 3α5βS is characterized by use-dependent antagonism and requires channel opening for inhibition (Petrovic et al., 2005; Borovska et al., 2012). When applied to preactivated receptors, DPA (2 μM) inhibited steady-state responses to 300 μM NMDA by 62.9 ± 1.9% (N = 3; Fig. 2A, left). Antagonism exhibited characteristic slow onset and offset. To test whether inhibition required channel opening, we preapplied DPA to closed NMDARs, followed by application of NMDA alone (Fig. 2A, right) (Borovska et al., 2012). Preapplication of DPA for 10 seconds inhibited peak responses to NMDA by 48.9 ± 2.0%, whereas steady-state current after preapplication of DPA was comparable with the steady-state current after coapplication of DPA and NMDA (111.2 ± 24.3%). Thus, although the shift in EC_{50} in Fig. 1B data could suggest a use-dependent (uncompetitive) mechanism of antagonism, these latter data suggest that DPA antagonism is not use dependent. We further examined the effect of 1 μM DPA on peak and steady-state NMDA currents when preapplied DPA was followed by coapplication with NMDA. DPA had similar effects on peak and steady-state NMDA current (Fig. 2B; 33.9 ± 3.4% inhibition of peak and 29.0 ± 12.9% inhibition of steady-state current; N = 5), again suggesting little or no dependence of antagonism on channel activation.

In contrast to results in Fig. 2A, the well characterized use-dependent channel blocker ketamine (2.5 μM) exhibited a requirement for channel activation (Fig. 2C). Application of ketamine (10 seconds) during NMDA application inhibited steady-state NMDA responses by 84.2 ± 2.9% (N = 3; Fig. 2C). When solely preapplied for the same amount of time, ketamine inhibited peak NMDA current by (26.9 ± 5.1%, Fig. 2C, dotted line), and steady-state responses were 635.9 ± 151.6% larger than currents following ketamine wash out during NMDA application (Fig. 2C, dashed line). The modest peak reduction is consistent with lipophilic retention of

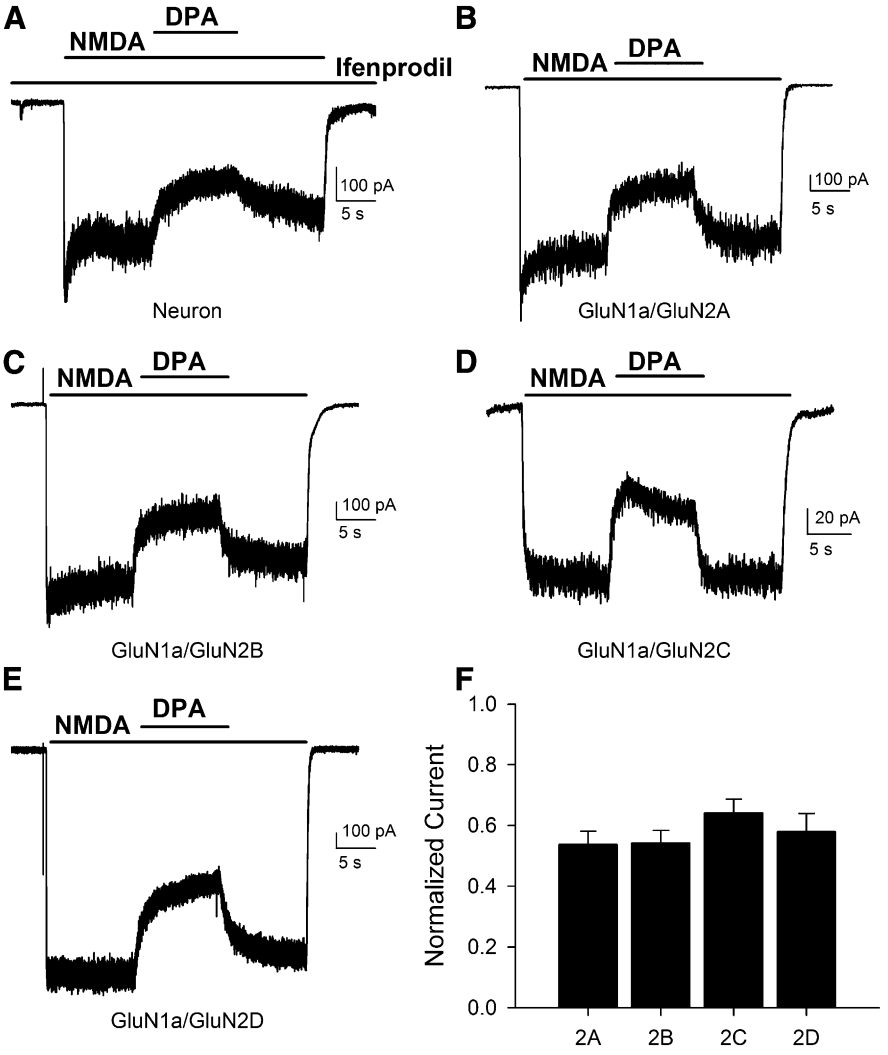

Fig. 3. Effects of DPA are independent of NMDA receptor subunit composition. (A) Current response to application of NMDA (300 μM), followed by coapplication with DPA (1 μM), and finally a return to NMDA alone in hippocampal neurons cotreated with ifenprodil (10 μM) to isolate responses from GluN2A subunit-containing receptors. (B–E) Similar current responses to NMDA with coapplication of DPA in HEK293 cells transfected with either GluN1a/GluN2A (B); GluN1a/GluN2B (C); GluN1a/GluN2C (D); or GluN1a/GluN2D (E). (F) Average degree of inhibition of NMDA-induced current (300 μM) by DPA (1 μM) in HEK293 cells transfected with either GluN2A, GluN2B, GluN2C, or GluN2D subunits (N = 6–10). Results were determined nonsignificant by one-way analysis of variance.

ketamine following aqueous removal (Orser et al., 1997), whereas the steady-state effects demonstrate clear activation dependence of ketamine onset and offset.

Cationic pore blockers like ketamine are characterized by "trapping" within the NMDAR ion channel, where offset of inhibition by the antagonist is accelerated in the presence of agonist (Mealing et al., 1999). To address whether DPA antagonism is affected similarly, DPA (3 μM) was applied to neurons after achieving steady-state NMDA current (300 μM) and then washed from the cell for 30 seconds in the presence of NMDA (Fig. 2D, top) or in the presence of saline (Fig. 2D, bottom) with brief pulses of NMDA to determine the degree of inhibition at two time points. At both points, the level of inhibition of NMDA current by DPA was similar (Fig. 2E), suggesting that the offset of inhibition by DPA is not affected by the presence of NMDA.

DPA is a Broad Spectrum NMDAR Antagonist. Some noncompetitive NMDAR antagonists exhibit subunit selectivity, making them valuable tools for the study of specific receptor populations in plasticity and other NMDAR functions. GluN2A and GluN2B are the major nonobligate NMDAR subunits in the hippocampus, whereas GluN2C and GluN2D are present in some hippocampal interneurons (Monyer et al., 1994). We examined subunit selectivity of DPA in hippocampal neurons using the GluN2B-selective blocker ifenprodil to isolate GluN2A-containing receptors (Fig. 3A). Ifenprodil (10 μM) blocks approximately one-half of the whole cell NMDA current under these conditions (Chang et al., 2010). DPA (1 μM) modulation of isolated GluN2A-containing receptors was similar to effects on the total population of receptors (0.63 $\pm$ 0.03; N = 5; compare with Fig. 1C). This result suggests that there is unlikely to be any selective effect of DPA on particular subunit combinations in native cells, although our results do not exclude selective effects on heterotrimeric receptors. The effect of DPA on the GluN2A population in hippocampal neurons appeared to be more potent than on these subunits expressed in oocytes (Fig. 1, A and B). HEK293 cells behaved more like neurons (Fig. 3), and there was no detectable difference in antagonism by a fixed DPA concentration among GluN1a/GluN2A, GluN1a/GluN2B, GluN1a/GluN2C, and GluN1a/GluN2D receptors (Fig. 3, B–F). These results suggest that DPA is a broad-spectrum NMDAR antagonist.

Some cationic NMDAR channel blockers may have selective actions on extrasynaptic NMDARs, a population that overlaps partially with GluN2B-containing receptors (Chen and Lipton, 1997; Tovar and Westbrook, 1999). After determining the degree of DPA-induced inhibition of NMDA current attributable to all NMDARs (Fig. 4A1), we enriched for extrasynaptic receptors by evoking autaptic NMDAR EPSCs in 10 μM MK-801, a slowly reversible, use-dependent channel blocker (Huettner and Bean, 1988). Following repeated stimulation, the EPSC was nearly abolished (Fig. 4A2), suggesting nearly full elimination of the synaptic receptor population. This MK-801 treatment depressed responses to exogenous NMDA by 75.5 $\pm$ 5.0% (Fig. 4A3; N = 4), consistent with previous estimates of the strong contribution of synaptic receptors to the total NMDAR pool (Rosenmund et al., 1995; Harris and Pettit, 2007; Wroge et al., 2012). We found that these NMDA responses, attributable mainly to extrasynaptic NMDARs, were inhibited by DPA (1 μM) similarly to the total NMDAR pool (Fig. 4B). Comparable results were obtained by incubating mass cultures in MK-801 to allow spontaneous synaptic activity to drive NMDAR block (data not shown). We used an MK-801 incubation protocol previously shown to block nearly all synaptic receptors in this preparation (Huettner and Bean, 1988; Hardingham et al., 2002; Wroge et al., 2012). Following MK-801 inhibition, extrasynaptic responses were inhibited 35.2 $\pm$ 4.4% by 1 μM DPA (N = 9, compare with Fig. 4B). Taken together, these two experiments suggest that DPA exhibits no selectivity for either synaptic or extrasynaptic NMDAR populations.

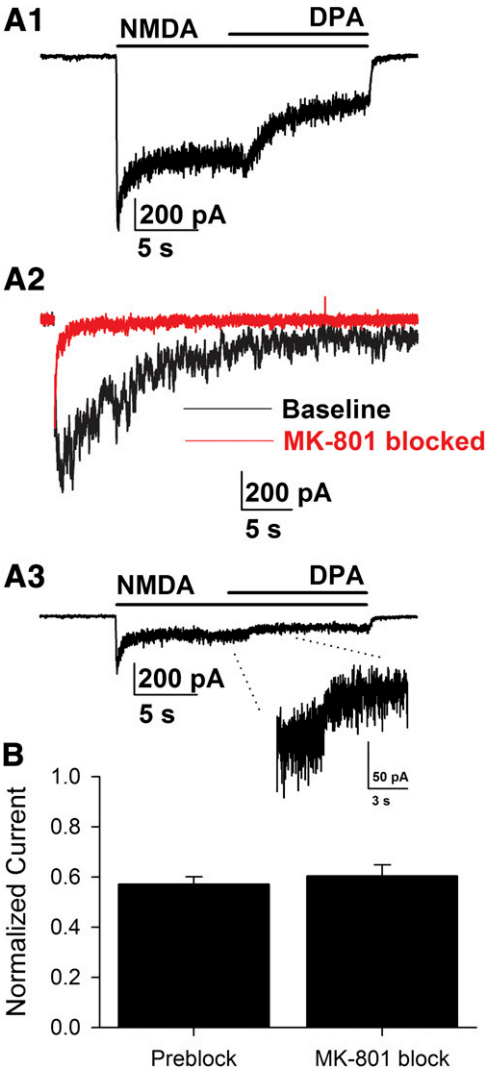

Fig. 4. Antagonism by DPA is similar at synaptic and extrasynaptic NMDARs. (A1) Response of a synaptically isolated hippocampal neuron grown on an astrocyte island to application of NMDA (300 μM) to all NMDARs, followed by coapplication with DPA (1 μM). (A2) Initial evoked autaptic EPSC (black) from the same cell, followed by EPSCs elicited in the presence of MK-801 (10 μM) until the EPSC was fully blocked (red). (A3) Current response to application of NMDA, then coapplication with DPA following MK-801-mediated removal of synaptic receptors. The inhibition of current by DPA is highlighted (inset). (B) Average normalized currents in DPA-treated cells before and after application of MK-801 (N = 4).

DPA Voltage Dependence. DPA exhibits well characterized, voltage-dependent translocation across the plasma membrane (Ketterer et al., 1971; Benz et al., 1976). Assuming DPA binds the NMDAR at a site within the plasma membrane, we sought to identify whether the binding site is

MOL PHARM
MOLECULAR PHARMACOLOGY
aspet

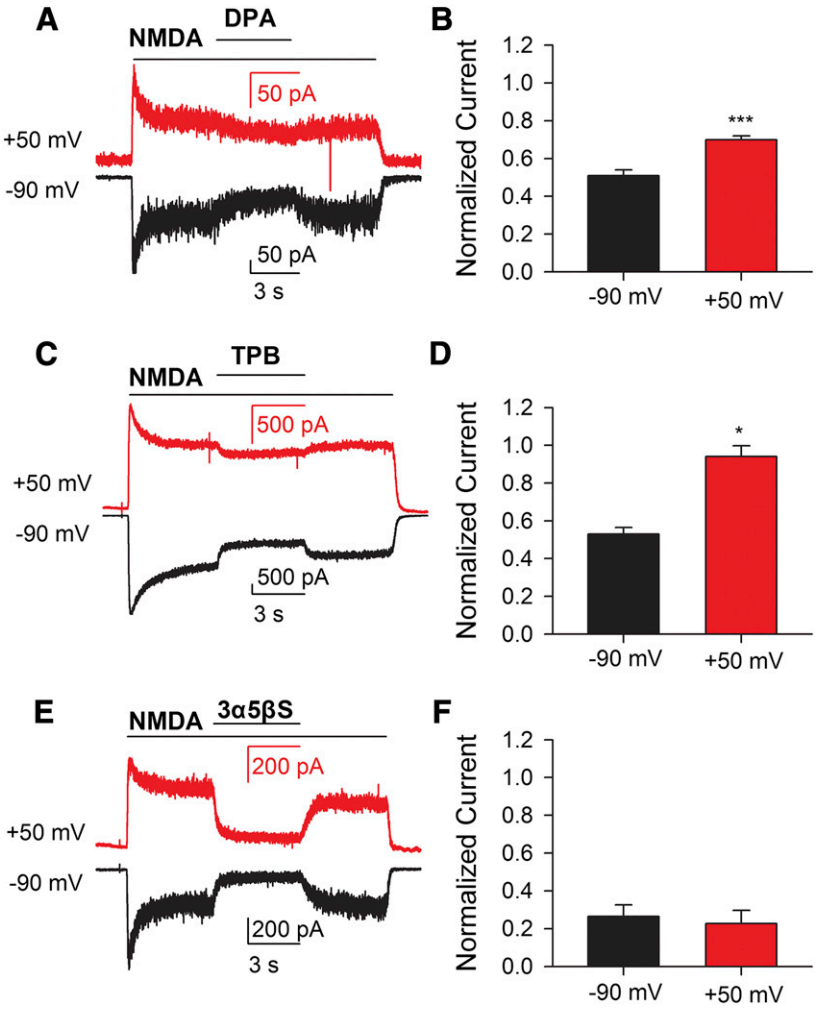

Fig. 5. DPA and TPB exert voltage-dependent antagonism, whereas 3α5βS does not. (A) Current responses at –90 mV (inward current, black) and +50 mV (outward current, red) of neurons administered NMDA (300 μM), then coapplied with DPA (1 μM), and finally a return to NMDA. (B) Average normalized NMDA-induced current by DPA at −90 mV and +50 mV holding membrane potentials (N = 11). (C) Current responses from a neuron challenged with NMDA (300 μM) and TPB (0.5 μM) and summary of normalized responses for TPB at −90 mV and +50 mV (D, N = 4). (E) Current responses for neurons treated with NMDA (300 μM) and 3α5βS (100 μM), as well as the summary of normalized current responses in presence of 3α5βS (F, N = 5). For (B) and (D) *$P < 0.05$; ***$P < 0.001$ by paired t-test compared with normalized current at −90 mV.

closer to the inner plasma membrane surface or to the external plasma membrane surface by examining the voltage dependence of DPA antagonism. Figure 5 shows DPA (1 μM) antagonism was significantly stronger at −90 mV than at +50 mV (Fig. 5, A and B). Another hydrophobic anion, tetraphenylborate (0.5 μM) showed a similar pattern of voltage dependence (Fig. 5, C and D). As expected, the sulfated steroid 3α5βS (100 μM) exhibited no voltage dependence (Fig. 5, E and F) (Park-Chung et al., 1994). Superficially, this voltage dependence by an anion is surprising because it mimics the effects of cationic channel blockers. Subsequent experiments were designed to elucidate potential mechanisms that may underlie the voltage dependence of DPA.

We performed voltage-pulse relaxation analysis of NMDA currents in the presence and absence of DPA to gain additional insight into the voltage dependence and time dependence of DPA's effects (Fig. 6). Small cells with limited neuritic arbors from young cultures (DIV 3-5) were used for these experiments to improve spatial clamp. Figure 6A shows families of responses to voltage pulses between −150 mV and +90 mV from a holding potential of −70 mV. Each family was generated by digitally subtracting a corresponding family of baseline traces, as defined in Fig. 6 legend. Figure 6A1 shows capacitive currents induced by DPA. As previously shown (Fernandez et al., 1983; Chisari et al., 2011), 1 μM DPA caused rapid, large capacitive currents in response to perturbations of the membrane potential. Figure 6A2 shows voltage-pulse responses obtained in the presence of 250 μM NMDA, after subtracting a family of responses in the absence of drugs. As previously reported, NMDARs exhibited weakly voltage-dependent gating in the nominal absence of Mg^{2+} (Clarke and Johnson, 2008) (Fig. 6A2). At the positive pulse potential of +90 mV, time-dependent outward current relaxation was evident. Rectification of steady-state responses and time-dependent outward relaxations became stronger in the presence of DPA (tail currents in Fig. 6A3). The family of currents in Fig. 6A3 was obtained by subtracting a family of currents in the presence of DPA alone from a family obtained in the combined presence of DPA and NMDA. Therefore, the capacitive effects of DPA shown in Fig. 6A1 were eliminated from Fig. 6A3. It can be appreciated that the outward current relaxations from inhibition at negative potentials to a new steady-state current level at positive potentials was substantially slower than the capacitive charge movements (Fig. 6A1), which reflect the translocation of DPA through the membrane. This suggests that DPA translocation is not directly linked to relief from antagonism at positive potentials. Relaxations upon return to the negative holding potential were also sometimes resolvable in subtractions (Fig. 6A3).

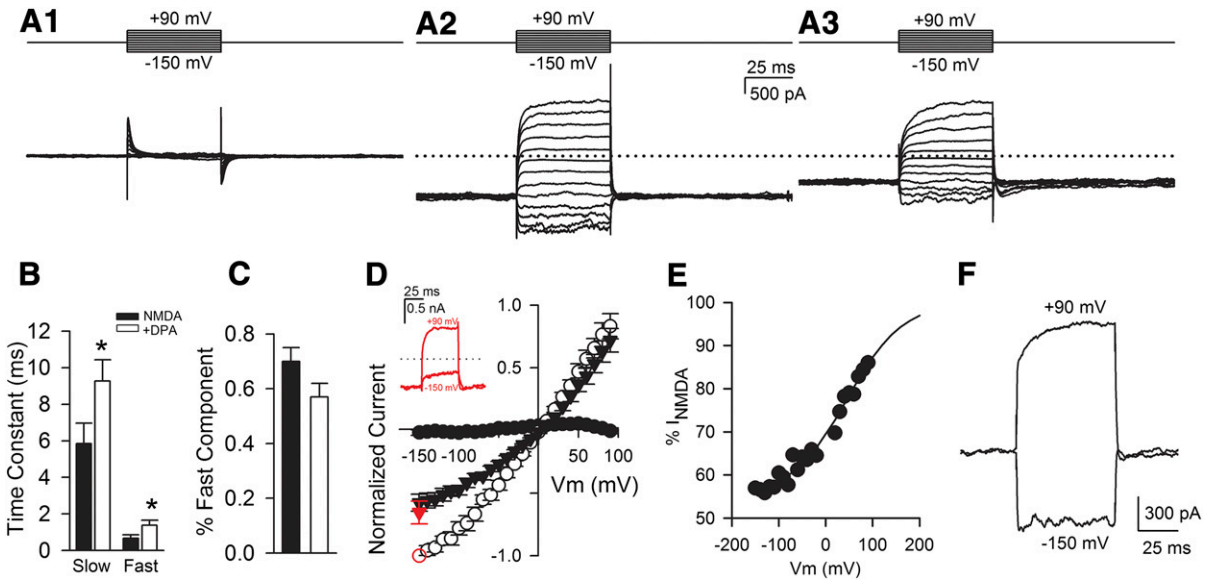

Fig. 6. Antagonism by DPA is voltage-dependent and slows voltage-dependent current relaxations. Hippocampal neurons were subjected to a voltage pulse protocol, stepping membrane voltage from −70 mV to a range of potentials between −150 mV and +90 mV in the presence of DPA (1 μM; A1), NMDA (250 μM; A2), or NMDA and DPA together (A3). Current responses prior to application of DPA or NMDA were digitally subtracted from the current responses during DPA or NMDA administration to generate the depicted representative traces. (B) Double-exponential fits were applied to subtracted traces after voltage jump from −70 mV to +90 mV. Depolarization-induced current relaxations were derived from the slow and fast components of the fit line ($N = 6$; $^*P < 0.05$ compared with NMDA alone). (C) The relative amplitude of the fast component from fits of current responses to voltage jumps from −70 mV to +90 mV ($N = 6$). There was only a trend-level change toward a less prominent fast component ($P > 0.05$). (D) The current-voltage relationship determined for DPA alone (closed circles), NMDA alone (open circles), or DPA coapplied with NMDA (closed triangles) from the voltage pulse protocol ($N = 10$). Normalized steady-state currents in the presence of 10 μM $MgCl_2$ are shown for pulses to −150 mV in red. Example current response to NMDA (250 μM) in the presence of $MgCl_2$ (10 μM) at −70 mV (holding), −150 mV, and +90 mV is shown (red inset) and demonstrates the negative slope conductance expected of Mg^{2+} block between −70 mV and −150 mV. Despite the Mg^{2+} inhibition of current at −150 mV, DPA antagonism was unaffected (red points on current-voltage curve; $N = 5$). (E) The mean percentage inhibition of control currents was plotted against holding potential and fit using a Boltzmann function (see *Materials and Methods*). Parameters of the Boltzmann fit are given in the *Results*. (F) Voltage-dependent current relaxation at +90 mV in the presence of NMDA (250 μM) and EDTA (0.1 mM). Baseline traces in the presence of EDTA only were subtracted.

The descriptions of relaxations in Fig. 6A, 2 and 3, are summarized in Fig. 6B. As previously documented, inherent voltage-dependent relaxations followed biexponential kinetics, (Fig. 6, B and C) (Clarke and Johnson, 2008). In the presence of DPA, relaxations still obeyed a biexponential time course. Rather than introducing a new component of relaxation, DPA slowed the two components (Fig. 6B), with no significant effect on the relative contribution of the fast component (Fig. 6C).

A summary current-voltage curve for steady-state currents obtained from the voltage-pulse protocol is shown in Fig. 6D and highlights the voltage-dependent nature of DPA-mediated inhibition relative to the inherent voltage dependence of steady-state NMDA currents. On the basis of Boltzmann analysis, the inhibition has a $V_{1/2}$ of 45.4 and a slope factor of 59.1 mV (corresponding to a calculated valence of 0.44; Fig. 6E). This voltage dependence is weaker than that describing translocation of DPA through the membrane bilayer of hippocampal neurons ($V_{1/2}$ of +13 mV and a slope factor of ~39 mV) (Chisari et al., 2011). These differences suggest that voltage dependence of NMDAR antagonism is unlikely to be associated directly with DPA's voltage-dependent translocation through the membrane bilayer.

To ensure that voltage dependence was observed across a range of DPA concentrations, we examined the effect of several DPA concentrations at −70 mV and at +40 mV within individual cells. We found that that the positive membrane potential weakened antagonism by DPA at all active concentrations tested (1, 3, and 10 μM) (data not shown; $P < 0.01$ by two-way ANOVA, $N = 5$). Although we found a main effect of both DPA concentration and voltage, there was no significant interaction, suggesting that depolarization decreased the effect of DPA similarly at each concentration.

Although the rectification of NMDA current in the absence of DPA in Fig. 6 matches that previously attributed to Mg^{2+}-independent rectification of gating (Clarke and Johnson, 2008), we cannot rule out a small effect of contaminating Mg^{2+}. Could DPA's voltage dependence arise from interaction with Mg^{2+} block? To test this possibility we added 10 μM Mg^{2+} to solutions. As expected, this introduced a region of negative slope conductance between −70 mV and −150 mV (Fig. 6D, inset). When 1 μM DPA inhibition was examined at −150 mV in the presence of this mild Mg^{2+} block, we found no evidence that the presence of Mg^{2+} interacted with DPA antagonism (Fig. 6D, red points). Arguing further that voltage-dependent current relaxations at +90 mV in nominally Mg^{2+}-free solutions did not result from Mg^{2+} contamination, we found that relaxations at +90 mV persisted in 0.1 mM disodium EDTA to chelate any residual Mg^{2+} (Fig. 6F; $N = 4$). DPA (1 μM) inhibition persisted in the presence of EDTA (42.3 ± 9.3% inhibition at −70 mV, $N = 4$). Because EDTA also chelates contaminating extracellular Zn^{2+} (Paoletti et al., 1997), this result also effectively excludes an interaction between DPA and Zn^{2+}.

To pursue further the hypothesis that membrane association does not directly underlie DPA's antagonism of NMDAR function, we compared the rate of DPA's absorption to the plasma membrane, measured as membrane capacitance increase, with its rate of interaction with NMDARs. Figure 7, A and B, shows both onset and offset of DPA antagonism during

the response to 300 μM NMDA. The early components of both onset and offset were adequately described by a single exponential function. Although both onset and offset of block also often appeared to exhibit a slow component, it was difficult to distinguish this slow component from the ongoing slow desensitization of receptors, so we did not include this element in our analysis (see Fig. 6A). Average onset and offset values for 1 μM DPA in this protocol were 381.7 $\pm$ 85.3 ms and 790.5 $\pm$ 174.9 ms, respectively (N = 7; Fig. 7E).

To monitor membrane interactions, we used repetitive, brief 20-mV voltage pulses from the holding potential of −70 mV and measured changes in membrane capacitance. We found that the interaction of DPA with the membrane exhibited an approximately 10-fold slower rate constant (Fig. 7, C–E) than the interaction of DPA with NMDARs. We previously showed that DPA-induced capacitance changes of membrane and antagonism of $GABA_AR$ function can be rapidly reversed by BSA application to the cells (Chisari et al., 2011). BSA is a well described scavenger of lipophilic agents (Richieri et al., 1993; Bojesen and Hansen, 2003). In contrast, we found that BSA had no significant effect on the fast time constant of antagonism offset at NMDARs, with 5-second application of 1 μM DPA (Fig. 7F). In sum, these data are consistent with the idea that DPA interacts directly with the NMDAR, at least at low concentrations, and that the effects of DPA on the plasma membrane play only an indirect role in antagonism.

Channel blockers such as memantine exhibit slowed dissociation from NMDARs at negative membrane potentials, accounting for the voltage dependence of steady-state inhibition (Gilling et al., 2009; MacDonald et al., 1987). We found that DPA (3 μM) exhibited qualitatively similar actions, where inhibition continued after ceasing application at −90 mV yet recovered at +50 mV (Fig. 8A). Again, this behavior is opposite of that predicted if membrane partitioning plays an important role in modulation of NMDARs. The offset

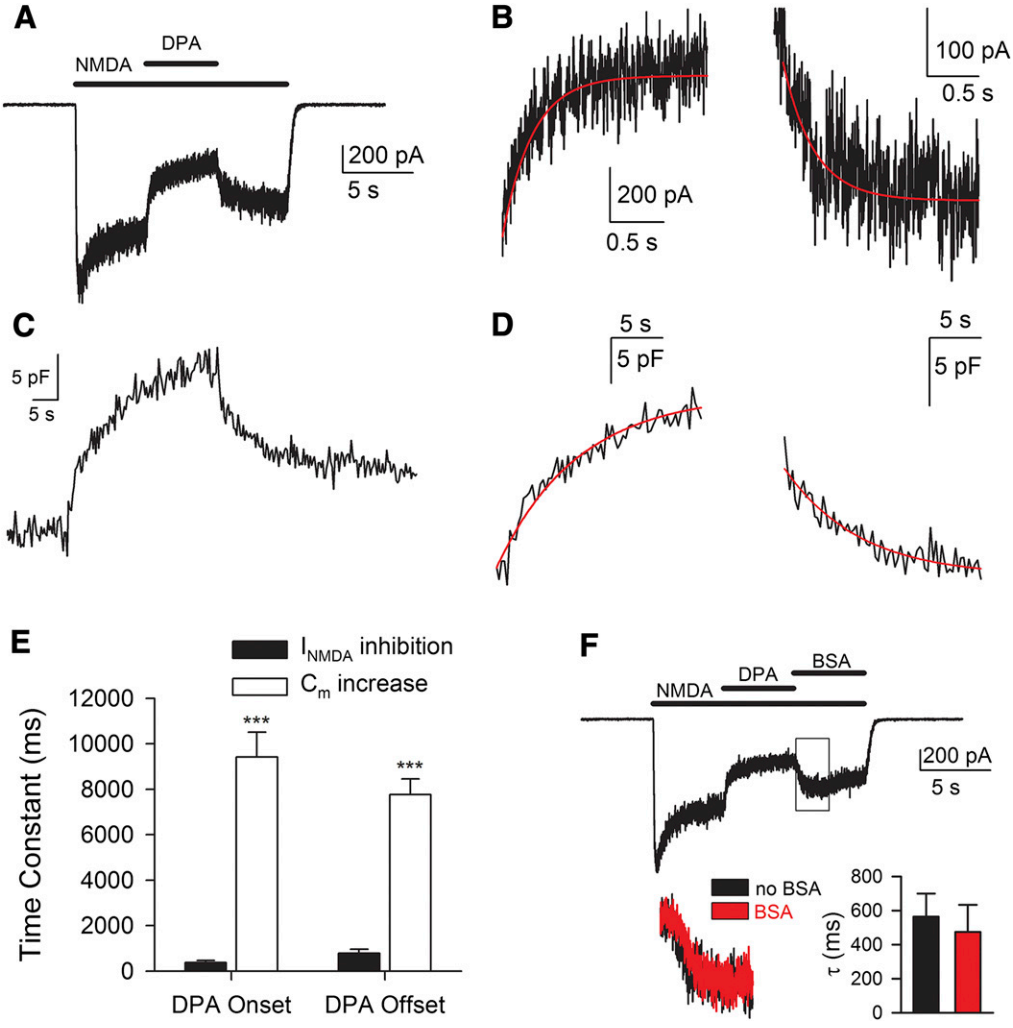

Fig. 7. NMDA receptor antagonism by DPA is independent of plasma membrane partitioning. (A) Current response to application of NMDA (300 μM), followed by coapplication with DPA (1 μM), and then a return to NMDA alone. (B) Exponential fits (red line) applied to onset and offset of DPA application. (C) Capacitance response to 30-second application of DPA (1 μM), followed by a return to saline (40 seconds). (D) Exponential fits (red line) applied to onset and offset of DPA application. (E) Time constants derived from calculated exponential fits were summarized for both NMDA-induced current inhibition (I_{NMDA} inhibition, N = 7) and increase in plasma membrane capacitance (C_m increase, N = 4). (F) Current response to application of NMDA (300 μM), followed by coapplication with DPA (1 μM), and then coapplication with BSA (0.1 mg/ml). Exponential fits were applied to offset of DPA in the presence or absence of BSA (bottom left) and found to be statistically nonsignificant (bottom right). For (E) ***$P < 0.001$ by unpaired t-test compared with I_{NMDA} inhibition.

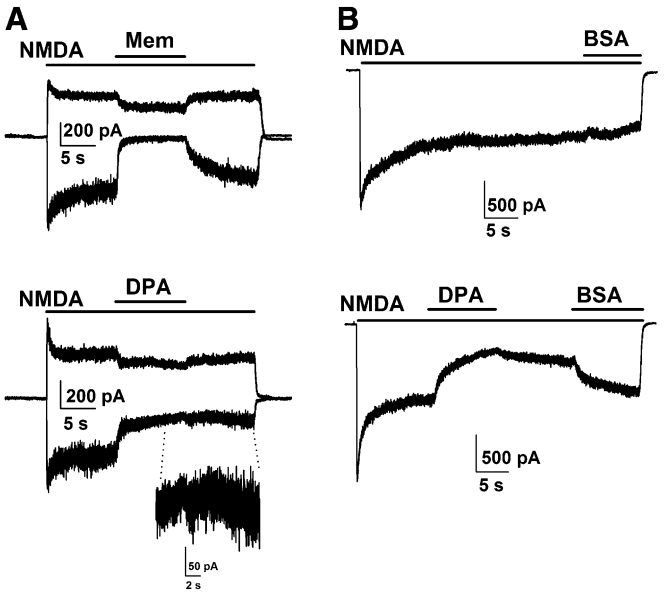

Fig. 8. DPA antagonism offset is slowed at negative membrane potentials. (A) Current responses at −90 mV (inward current) and +50 mV (outward current) to application of NMDA (300 μM), followed by coapplication with either memantine (10 μM, top) or DPA (3 μM, bottom), and then a return to NMDA alone. In both cases, antagonism offset at the positive potential is faster than at the negative potential. The offset of DPA at −90 mV is shown enlarged (inset). (B) Current responses at −90 mV to application of NMDA (300 μM) in the absence (top) and presence (bottom) of DPA (3 μM), followed by a return to NMDA alone, and then coapplication with BSA (0.1 mg/ml).

of NMDAR antagonism by memantine (10 μM) was faster at +50 mV than at −90 mV (the calculated time constants were 610.8 ± 127.6 ms at +50 mV and 2929.2 ± 1058.6 ms at −90 mV; N = 4–7). Alternatively, the offset of DPA's NMDAR antagonism at +50 mV appeared qualitatively faster than at −90 mV (the calculated time constant was 2703.1 ± 545.1 ms at +50 mV; exponential fits could not be calculated at −90 mV with the same wash period; N = 5). This is in contrast to effects of DPA on $GABA_A$Rs, where offset of DPA antagonism is dramatically slowed at positive membrane potentials (Chisari et al., 2011). On the other hand, we observed that at these high concentrations of DPA (3 μM), BSA speeded recovery from antagonism (Fig. 8B), consistent with the idea that membrane-retained DPA has indirect access to the NMDAR.

We hypothesized that the counterintuitive voltage dependence of antagonism by an anion, and the behavior that contradicts actions at $GABA_A$Rs, could be explained if outer membrane-associated DPA, but not inner-surface DPA, can access the NMDAR antagonism site. Because inner-membrane surface DPA (favored at positive membrane potentials) is resistant to washout (Chisari et al., 2011), we reasoned that antagonism might be restored following washout of DPA at +50 mV by stepping the membrane potential back to −90 mV, as trapped inner-membrane surface DPA translocates back to the outer membrane surface (Fig. 9, A and B). In contrast to this prediction, we found that following DPA application at +50 mV (Fig. 9C), NMDA currents were not significantly inhibited following return to −90 mV, measured 5 seconds following DPA washout and 5 seconds following repolarization. Alternatively, DPA applied at −90 mV on the same cells exhibited protracted antagonism following washout (Fig. 9, D and E), as observed in the protocol in Fig. 8. This is in direct contrast to the pattern of membrane retention detected as membrane capacitance increases (Fig. 9, F and G), which verified trapping of DPA in the membrane at +50 mV. DPA applied at +50 mV and washed away at +50 mV yielded larger capacitance increases than DPA washed on and off at a membrane potential of −90 mV throughout (Fig. 9H). This pattern of results demonstrates that DPA trapped in the membrane at +50 mV and subsequently returned to the outer leaflet cannot significantly interact with NMDARs. Thus, the pool of DPA detectable electrically by capacitance measurements does not have direct access to the NMDAR. We conclude that voltage dependence of DPA does not arise by access to a site associated with the outer membrane leaflet.

Voltage-dependent channel blockers like ketamine and Mg^{2+} exhibit sensitivity to the direction of current flow (MacDonald et al., 1987; MacDonald and Nowak, 1990). Dissociation is accelerated and steady-state block is decreased by outward current at positive potentials (Chen and Lipton, 1997; Mennerick et al., 1998). If DPA binds residues near the channel mouth, perhaps voltage dependence could be imparted to DPA actions through a similar interaction with permeant ions. To test whether DPA is also sensitive to the direction of current flow, we altered the reversal potential for NMDAR currents using a choline-rich whole cell pipette solution. Under these conditions, reversal of currents occurs at approximately +50 mV instead of 0 mV, and Mg^{2+} block but not DPA antagonism significantly increased (Fig. 10). This result shows that voltage dependence is not derived from permeant ion interaction with DPA and verifies that DPA is unlikely to act through channel block.

Discussion

Our study establishes DPA as a unique anionic, noncompetitive, and voltage-dependent NMDAR antagonist. Antagonism has a number of attributes distinct from modulation of NMDARs by channel blockers and distinct from actions of other negatively charged NMDAR antagonists. Antagonism is also fundamentally different from actions of DPA at $GABA_A$Rs.

In part, we examined DPA because of its similarity at $GABA_A$Rs to sulfated neurosteroids, which also modulate NMDARs. DPA has superficially similar physicochemical properties to sulfated steroids (hydrophobicity, negative charge). Some sulfated neurosteroids positively regulate NMDARs; others negatively regulate (Weaver et al., 2000). DPA exhibits potency at least 10 times greater than steroid inhibitors at NMDARs, and its effective concentration range is similar to widely used antagonists (low micromolar). Additionally, antagonism by some sulfated steroids is use dependent (Petrovic et al., 2005), and the voltage dependence of DPA appears to be distinct from actions of neurosteroids (Park-Chung et al., 1997; Petrovic et al., 2005). These differences from neurosteroids may suggest a different site of interaction for DPA. However, because the amino acid residues responsible for steroid antagonism remain unclear (Gibbs et al., 2006), it is difficult to test directly the similarity of mechanisms underlying neurosteroid and DPA modulation. GluN2C/D-containing receptors are somewhat more sensitive to sulfated steroid antagonism than GluN2A/B NMDARs (Malayev et al., 2002; Horak et al., 2006). However, in experiments shown in this study, GluN2C and GluN2D

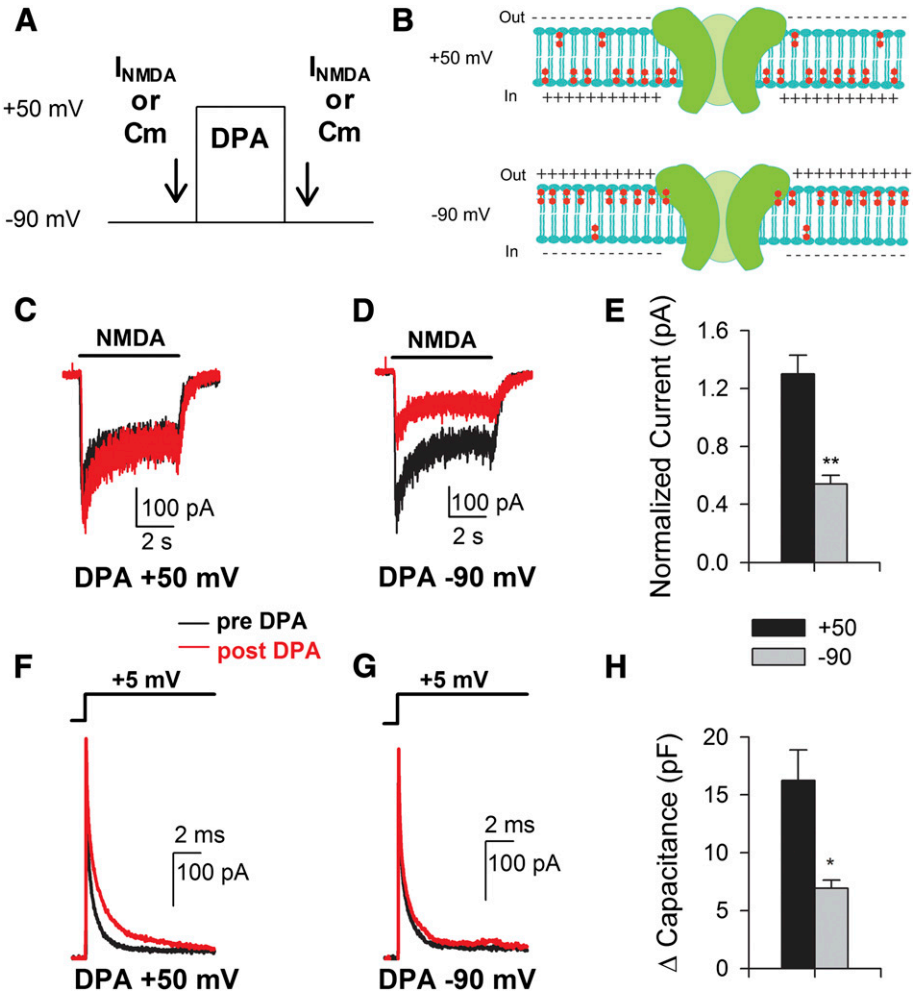

Fig. 9. Membrane retention of DPA does not account for inhibition of NMDA current. (A) Schematized protocol used in these experiments. NMDA current (I_{NMDA}) or membrane capacitance (Cm) was measured before and after DPA application at either +50 mV or −90 mV. The arrows represent the relative time point when the measurement was taken at −90 mV. (B) A diagram illustrating the relative distribution in the plasma membrane of DPA molecules (red) at +50 mV (top) and −90 mV (bottom). The illustration includes a representation of an NMDA receptor (green). (C and D) Current responses to application of NMDA (300 μM) at −90 mV before (black trace) and after (red trace) a 10-second application of DPA (3 μM; followed by 5-second washout) at either +50 mV (C) or −90 mV (D). (E) Summary of change in NMDA current for the protocols shown in (C) and (D) (red trace normalized to black trace; N = 5). (F and G) to monitor membrane retention, we performed a similar DPA application protocol at two membrane potentials but measured membrane capacitance. We delivered a +5-mV pulse at a holding potential of −90 mV before (black line) and after application of DPA (3 μM, red line) to monitor capacitive current. DPA was applied for 10 seconds (followed by 5-second washout) at +50 mV (F) or at −90 mV (G). There was stronger retention of DPA-induced membrane capacitance when DPA was applied at +50 mV (H, N = 4). Thus, although DPA is retained in the membrane longer at +50 mV, it is retained on receptors longer at −90 mV. For (E and H) $^*P < 0.05$; $^{**}P < 0.01$ by paired t-test compared with application at +50 mV.

sensitivities to DPA inhibition did not differ from GluN2A/B subunits, suggesting that DPA's mechanism of antagonism differs from sulfated neurosteroids.

Superficially, the effects of DPA resemble those of cationic open channel antagonists including clinically and experimentally interesting compounds like memantine, ketamine, PCP, and MK-801. These primarily include the noncompetitive profile (Fig. 1) and voltage dependence of antagonism offset (Fig. 8). Clearly it is difficult to envision how anionic DPA could act by a similar mechanism as cationic pore blockers. Indeed, DPA distinguishes itself from these blockers by the lack of requirement for channel opening (Fig. 2), much weaker voltage dependence (Fig. 5), and insensitivity to driving force on permeant ions (Fig. 10).

DPA antagonism of NMDARs also differs in important ways from DPA interactions with $GABA_A$Rs (Chisari et al., 2011). DPA exhibits higher potency at $GABA_A$Rs (IC_{50} of 0.065 μM at GABA EC_{90}) than at NMDARs (IC_{50} of 2.3 μM at NMDA EC_{90}). Also, block of $GABA_A$Rs exhibits clear activation dependence whereas antagonism of NMDARs does not. Finally, steady-state $GABA_A$R antagonism by DPA exhibits no detectable dependence on membrane potential. However, offset of DPA antagonism at $GABA_A$Rs is strongly voltage dependent and matches the strong membrane retention of DPA at positive membrane potentials, assessed both by fluorescence resonance energy transfer interactions with DiO and by membrane capacitance measurements (Chisari et al., 2011). This is precisely the opposite of DPA's effects on NMDARs. Instead, offset of DPA NMDAR antagonism was faster at positive potentials than at negative potentials (Fig. 8), and antagonism exhibited no resurgence upon return to a negative potential, despite demonstrable, strong membrane retention of DPA (Fig. 9). We conclude that the pool of DPA responsible for capacitive currents is not directly responsible for NMDAR antagonism.

At present we cannot exclude multiple sites for interaction of DPA with NMDARs, which could include an aqueous accessible site and sites that require membrane partitioning. Our observations are most consistent with the idea of a drug-receptor interaction from the aqueous phase (Fig. 7). However, experiments represented in Fig. 8 suggest that offset/recovery times vary with concentration of DPA, which is not expected from canonical drug-receptor interactions. Thus, DPA may access inhibitory sites from both the aqueous and lipid phases, possibly indicating more than one binding site.

If the voltage dependence of DPA antagonism does not arise from its voltage-dependent translocation through the membrane or from channel block, then what accounts for the sensitivity to membrane potential (Nowak et al., 1984; Ascher and Nowak, 1988; Clarke and Johnson, 2008)? One possibility is that the key to voltage dependence lies in the inherent rectification of NMDAR gating (Jahr and Stevens, 1990;

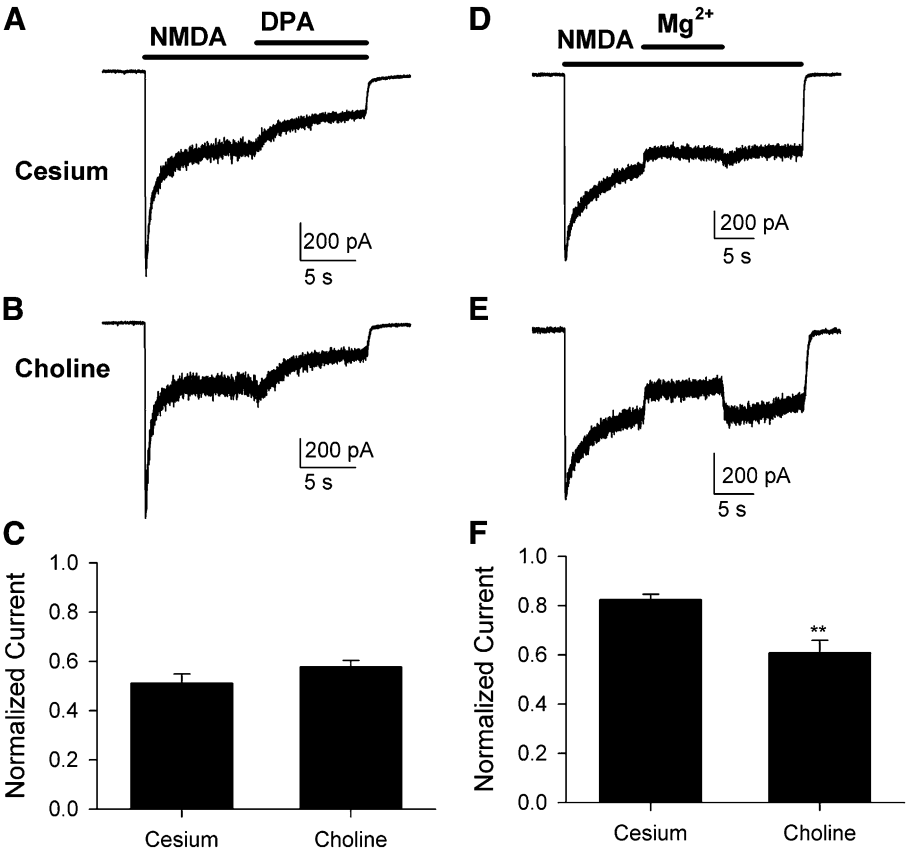

Fig. 10. Increasing driving force does not affect antagonism by DPA. Current responses to application of NMDA (300 μM), followed by coapplication with either DPA (1 μM; A and B) or Mg^{2+} (100 μM; D and E). For both antagonists, experiments were performed using either a cesium-based (A and D) or a choline-based (B and E) pipette solution to manipulate the reversal potential and increase the inward driving force of permeant ions through the NMDAR channel. Although no significant difference between the two pipette solutions was observed during antagonism by DPA (C; $N = 5$), the choline-based internal solution significantly increased antagonism by Mg^{2+} (F; $N = 5$–6). $^{**}P < 0.01$ by unpaired t-test compared with CsCl internal solution. Holding potential was −60 mV.

Clarke and Johnson, 2008; Yang et al., 2010), which could include Ca^{2+} dependent desensitization (Clark et al., 1990; Tong et al., 1995). Although this explanation for voltage dependence remains speculative, perhaps DPA interacts with conformations of the channel favored at negative membrane potentials to reduce channel opening. Future single-channel studies could test this hypothesis.

In summary, we characterized a distinct form of negative NMDAR modulation by a hydrophobic anion used for many years in classic biophysical studies. Although actions are less potent than DPA inhibition of $GABA_A$Rs, potency at NMDA receptors is similar to many widely used NMDAR antagonists. Antagonism of both receptor types should be considered and accounted for in studies of cellular excitability. Pharmacologically, DPA exhibits unusual voltage dependence at NMDARs that is surprisingly similar qualitatively to the effects of cationic channel blockers.

Acknowledgments

The authors thank Ann Benz and Amanda Taylor for technical help with cultures. The authors also thank laboratory members and Larry Eisenman for discussion. The authors thank Peter Seeburg (Max Plank Institute) and Stephen Traynelis and Kasper Hansen (Emory University) for the kind gifts of GluN subunits.

Authorship Contributions

Participated in research design: Linsenbardt, Chisari, Mennerick.
Conducted experiments: Linsenbardt, Chisari, Shu, Yu.
Performed data analysis: Linsenbardt, Chisari, Yu, Mennerick.
Wrote or contributed to the writing of the manuscript: Linsenbardt, Chisari, Zorumski, Mennerick.

References

Anderson CR and Stevens CF (1973) Voltage clamp analysis of acetylcholine produced end-plate current fluctuations at frog neuromuscular junction. *J Physiol* **235**:655–691.
Antonov SM, Gmiro VE, and Johnson JW (1998) Binding sites for permeant ions in the channel of NMDA receptors and their effects on channel block. *Nat Neurosci* **1**: 451–461.
Antonov SM and Johnson JW (1999) Permeant ion regulation of N-methyl-D-aspartate receptor channel block by Mg(2+). *Proc Natl Acad Sci USA* **96**: 14571–14576.
Ascher P and Nowak L (1988) The role of divalent cations in the N-methyl-D-aspartate responses of mouse central neurones in culture. *J Physiol* **399**: 247–266.
Benz R, Läuger P, and Janko K (1976) Transport kinetics of hydrophobic ions in lipid bilayer membranes. Charge-pulse relaxation studies. *Biochim Biophys Acta* **455**: 701–720.
Boeckman FA and Aizenman E (1996) Pharmacological properties of acquired excitotoxicity in Chinese hamster ovary cells transfected with N-methyl-D-aspartate receptor subunits. *J Pharmacol Exp Ther* **279**:515–523.
Bojesen IN and Hansen HS (2003) Binding of anandamide to bovine serum albumin. *J Lipid Res* **44**:1790–1794.
Borovska J, Vyklicky V, Stastna E, Kapras V, Slavikova B, Horak M, Chodounska H, and Vyklicky L, Jr (2012) Access of inhibitory neurosteroids to the NMDA receptor. *Br J Pharmacol* **166**:1069–1083.
Boulter J, Hollmann M, O'Shea-Greenfield A, Hartley M, Deneris E, Maron C, and Heinemann S (1990) Molecular cloning and functional expression of glutamate receptor subunit genes. *Science* **249**:1033–1037.
Bradley J, Luo R, Otis TS, and DiGregorio DA (2009) Submillisecond optical reporting of membrane potential in situ using a neuronal tracer dye. *J Neurosci* **29**: 9197–9209.
Chanda B, Asamoah OK, Blunck R, Roux B, and Bezanilla F (2005a) Gating charge displacement in voltage-gated ion channels involves limited transmembrane movement. *Nature* **436**:852–856.
Chanda B, Blunck R, Faria LC, Schweizer FE, Mody I, and Bezanilla F (2005b) A hybrid approach to measuring electrical activity in genetically specified neurons. *Nat Neurosci* **8**:1619–1626.
Chang CY, Jiang X, Moulder KL, and Mennerick S (2010) Rapid activation of dormant presynaptic terminals by phorbol esters. *J Neurosci* **30**:10048–10060.
Chen HS and Lipton SA (1997) Mechanism of memantine block of NMDA-activated channels in rat retinal ganglion cells: uncompetitive antagonism. *J Physiol* **499**: 27–46.
Chisari M, Wu K, Zorumski CF, and Mennerick S (2011) Hydrophobic anions potently and uncompetitively antagonize GABA(A) receptor function in the absence of a conventional binding site. *Br J Pharmacol* **164** (2b):667–680.

Clark GD, Clifford DB, and Zorumski CF (1990) The effect of agonist concentration, membrane voltage and calcium on N-methyl-D-aspartate receptor desensitization. *Neuroscience* **39**:787–797.
Clarke RJ and Johnson JW (2008) Voltage-dependent gating of NR1/2B NMDA receptors. *J Physiol* **586**:5727–5741.
Collingridge GL, Isaac JT, and Wang YT (2004) Receptor trafficking and synaptic plasticity. *Nat Rev Neurosci* **5**:952–962.
Dingledine R, Borges K, Bowie D, and Traynelis SF (1999) The glutamate receptor ion channels. *Pharmacol Rev* **51**:7–61.
Fernández JM, Taylor RE, and Bezanilla F (1983) Induced capacitance in the squid giant axon. Lipophilic ion displacement currents. *J Gen Physiol* **82**:331–346.
Gibbs TT, Russek SJ, and Farb DH (2006) Sulfated steroids as endogenous neuromodulators. *Pharmacol Biochem Behav* **84**:555–567.
Gilling KE, Jatzke C, Hechenberger M, and Parsons CG (2009) Potency, voltage-dependency, agonist concentration-dependency, blocking kinetics and partial untrapping of the uncompetitive N-methyl-D-aspartate (NMDA) channel blocker memantine at human NMDA (GluN1/GluN2A) receptors. *Neuropharmacology* **56**:866–875.
Hardingham GE, Fukunaga Y, and Bading H (2002) Extrasynaptic NMDARs oppose synaptic NMDARs by triggering CREB shut-off and cell death pathways. *Nat Neurosci* **5**:405–414.
Harris AZ and Pettit DL (2007) Extrasynaptic and synaptic NMDA receptors form stable and uniform pools in rat hippocampal slices. *J Physiol* **584**:509–519.
Horak M, Vlcek K, Chodounska H, and Vyklicky L, Jr (2006) Subtype-dependence of N-methyl-D-aspartate receptor modulation by pregnenolone sulfate. *Neuroscience* **137**:93–102.
Huettner JE and Bean BP (1988) Block of N-methyl-D-aspartate-activated current by the anticonvulsant MK-801: selective binding to open channels. *Proc Natl Acad Sci USA* **85**:1307–1311.
Jahr CE and Stevens CF (1990) A quantitative description of NMDA receptor-channel kinetic behavior. *J Neurosci* **10**:1830–1837.
Jin X, Covey DF, and Steinbach JH (2009) Kinetic analysis of voltage-dependent potentiation and block of the glycine alpha 3 receptor by a neuroactive steroid analogue. *J Physiol* **587**:981–997.
Kashiwagi K, Masuko T, Nguyen CD, Kuno T, Tanaka I, Igarashi K, and Williams K (2002) Channel blockers acting at N-methyl-D-aspartate receptors: differential effects of mutations in the vestibule and ion channel pore. *Mol Pharmacol* **61**:533–545.
Ketterer B, Neumcke B, and Läuger P (1971) Transport mechanism of hydrophobic anions through lipid bilayer membranes. *J Membr Biol* **5**:225–245.
Lu W, Man H, Ju W, Trimble WS, MacDonald JF, and Wang YT (2001) Activation of synaptic NMDA receptors induces membrane insertion of new AMPA receptors and LTP in cultured hippocampal neurons. *Neuron* **29**:243–254.
MacDonald JF, Miljkovic Z, and Pennefather P (1987) Use-dependent block of excitatory amino acid currents in cultured neurons by ketamine. *J Neurophysiol* **58**:251–266.
MacDonald JF and Nowak LM (1990) Mechanisms of blockade of excitatory amino acid receptor channels. *Trends Pharmacol Sci* **11**:167–172.
Malayev A, Gibbs TT, and Farb DH (2002) Inhibition of the NMDA response by pregnenolone sulphate reveals subtype selective modulation of NMDA receptors by sulphated steroids. *Br J Pharmacol* **135**:901–909.
Mealing GA, Lanthorn TH, Murray CL, Small DL, and Morley P (1999) Differences in degree of trapping of low-affinity uncompetitive N-methyl-D-aspartic acid receptor antagonists with similar kinetics of block. *J Pharmacol Exp Ther* **288**:204–210.
Mennerick S, Jevtovic-Todorovic V, Todorovic SM, Shen W, Olney JW, and Zorumski CF (1998) Effect of nitrous oxide on excitatory and inhibitory synaptic transmission in hippocampal cultures. *J Neurosci* **18**:9716–9726.
Mennerick S, Que J, Benz A, and Zorumski CF (1995) Passive and synaptic properties of hippocampal neurons grown in microcultures and in mass cultures. *J Neurophysiol* **73**:320–332.
Monyer H, Burnashev N, Laurie DJ, Sakmann B, and Seeburg PH (1994) Developmental and regional expression in the rat brain and functional properties of four NMDA receptors. *Neuron* **12**:529–540.
Nakazawa K, McHugh TJ, Wilson MA, and Tonegawa S (2004) NMDA receptors, place cells and hippocampal spatial memory. *Nat Rev Neurosci* **5**:361–372.
Nowak L, Bregestovski P, Ascher P, Herbet A, and Prochiantz A (1984) Magnesium gates glutamate-activated channels in mouse central neurones. *Nature* **307**:462–465.
Nowak LM and Wright JM (1992) Slow voltage-dependent changes in channel open-state probability underlie hysteresis of NMDA responses in Mg(2+)-free solutions. *Neuron* **8**:181–187.
Orser BA, Pennefather PS, and MacDonald JF (1997) Multiple mechanisms of ketamine blockade of N-methyl-D-aspartate receptors. *Anesthesiology* **86**:903–917.
Paoletti P, Ascher P, and Neyton J (1997) High-affinity zinc inhibition of NMDA NR1-NR2A receptors. *J Neurosci* **17**:5711–5725.
Park-Chung M, Wu FS, and Farb DH (1994) 3 alpha-Hydroxy-5 beta-pregnan-20-one sulfate: a negative modulator of the NMDA-induced current in cultured neurons. *Mol Pharmacol* **46**:146–150.
Park-Chung M, Wu FS, Purdy RH, Malayev AA, Gibbs TT, and Farb DH (1997) Distinct sites for inverse modulation of N-methyl-D-aspartate receptors by sulfated steroids. *Mol Pharmacol* **52**:1113–1123.
Petrovic M, Sedlacek M, Horak M, Chodounska H, and Vyklický L, Jr (2005) 20-oxo-5beta-pregnan-3alpha-yl sulfate is a use-dependent NMDA receptor inhibitor. *J Neurosci* **25**:8439–8450.
Richieri GV, Anel A, and Kleinfeld AM (1993) Interactions of long-chain fatty acids and albumin: determination of free fatty acid levels using the fluorescent probe ADIFAB. *Biochemistry* **32**:7574–7580.
Rosenmund C, Feltz A, and Westbrook GL (1995) Synaptic NMDA receptor channels have a low open probability. *J Neurosci* **15**:2788–2795.
Sobolevsky AI, Koshelev SG, and Khodorov BI (1999) Probing of NMDA channels with fast blockers. *J Neurosci* **19**:10611–10626.
Tong G, Shepherd D, and Jahr CE (1995) Synaptic desensitization of NMDA receptors by calcineurin. *Science* **267**:1510–1512.
Tovar KR and Westbrook GL (1999) The incorporation of NMDA receptors with a distinct subunit composition at nascent hippocampal synapses in vitro. *J Neurosci* **19**:4180–4188.
Weaver CE, Land MB, Purdy RH, Richards KG, Gibbs TT, and Farb DH (2000) Geometry and charge determine pharmacological effects of steroids on N-methyl-D-aspartate receptor-induced Ca(2+) accumulation and cell death. *J Pharmacol Exp Ther* **293**:747–754.
Weiss DS (1988) Membrane potential modulates the activation of GABA-gated channels. *J Neurophysiol* **59**:514–527.
Woodhull AM (1973) Ionic blockage of sodium channels in nerve. *J Gen Physiol* **61**:687–708.
Wroge CM, Hogins J, Eisenman L, and Mennerick S (2012) Synaptic NMDA receptors mediate hypoxic excitotoxic death. *J Neurosci* **32**:6732–6742.
Yang YC, Lee CH, and Kuo CC (2010) Ionic flow enhances low-affinity binding: a revised mechanistic view into Mg2+ block of NMDA receptors. *J Physiol* **588**:633–650.

Address correspondence to: Steven Mennerick, Departments of Psychiatry and Anatomy & Neurobiology, Washington University School of Medicine, 660 S. Euclid Ave., Box 8134, St. Louis, MO 63110. E-mail: menneris@wustl.edu